

# Stress and input energy analyses of shearing a particle bed under a centrifugal field

Sadegh Nadimi<sup>a,b,\*</sup>, Mojtaba Ghadiri<sup>a</sup>

<sup>a</sup> Faculty of Engineering, University of Leeds, UK

<sup>b</sup> School of Engineering, Newcastle University, UK

## ARTICLE INFO

### Article history:

Received 3 September 2020

Received in revised form 22 August 2021

Accepted 26 August 2021

Available online 01 September 2021

### Keywords:

Discrete element method

DEM

Mechanofusion

Particle dynamics

Stress analysis

Energy input

## ABSTRACT

Effective shearing of fine powders for surface modification and dry coating requires a compressed powder bed to prevent aeration. A device known as Mechanofusion® provides the necessary conditions using a centrifugal field, under which submicron particles are coated onto coarser host particles by shearing under great compressive forces at very high strain rates. This creates composite powders with enhanced properties, such as good flowability, surface functional effects, etc. Understanding the dynamics of particle motion, required level of shear stresses and input energy is a prerequisite for process optimisation. Here, numerical simulation by the Discrete Element Method is carried out, analysing features which are otherwise difficult to obtain by experimental work, e.g. the determination of the thickness of the zone in which particles experience shearing strains, as necessary for functional effect, compressive forces on particles, and input energy. Correlations are proposed for the energy input requirement and stresses experienced by the device as a function of rotational speed.

© 2021 The Authors. Published by Elsevier B.V. This is an open access article under the CC BY license (<http://creativecommons.org/licenses/by/4.0/>).

## 1. Introduction

Dry coating and surface modification of fine powders are challenging as the bulk powder readily aerates, making it difficult to shear the particles under large stresses to smear the surfaces with other powders of interest. Yokoyama et al. [1] developed a device called the Angmill Mechanofusion system, employing a centrifugal field to compress the fine powder, thus making it possible to shear the bulk powder for surface modification and dry coating of micrometre size powder with finer powders for fusion or dry lubrication. Several new versions of this device are available commercially, known as Mechanofusion®. This device consists of a rotating cylindrical chamber, in which a fixed rounded inner-piece, called push-arm, and a fixed scraper blade are placed. When the chamber is rotated, high centrifugal forces are exerted on the particle bed, causing it to undergo compression against the chamber wall. While passing through an adjustable gap between the push-arm and chamber wall, extreme shear straining takes place under large compression loads. The particulate bed continuously undergoes this process while the chamber is rotating. The forces acting on the particles are very large and may alter the physical and chemical characteristics of the powder. The frictional forces may cause heat and plastic deformation. As a result of high compressive and shear forces, the fusion between the particles might be induced. The device is used

in a number of applications, for example in pharmaceuticals for providing a uniform distribution of active ingredients over the surfaces of carrier particles, dry coating by lubricants and mechanochemistry for enhancing the solubility of tablet components [2, 3]. Its extreme mixing conditions provide homogeneity and strength for colouring of pigments [4]. Its use has also been suggested for preparation of cathode materials in battery industry [5] and applications in cosmetics [6].

The application of Mechanofusion for particle surface modification has been reported by Koishi et al. [7]; Alonso et al. [8]; Tanno [9] and Naito et al. [10]. Yokoyama et al. [1] investigated the combination of more than 100 different host and guest particles by this process. Alonso et al. [8] noted the size reduction of the guest powder agglomerate took place in this device and the host particle surface texture was highly modified with a partial penetration of the fine component into the body of the larger particles. Herman et al. [11] reported that the Mechanofusion system could perform size reduction and shape spherulisation for brittle and irregularly shaped powders. They observed a significant improvement in powder flow characteristics.

There are only few studies addressing the analysis of the Mechanofusion system. An early work by Chen et al. [12] proposed a preliminary model of the Mechanofusion system and developed quantitative relationships among system variables and their effects. Pfeffer et al. [13], Dave et al. [14] and Chen et al. [15] have analysed a small scale system using two-dimensional (2D) Discrete Element Method (DEM) simulations, investigating the nature of inter-particle forces generated due to the action of the push-arm and the scraper as the rotating chamber is spinning at various speeds.

\* Corresponding author at: 2.18 Drummond Building, School of Engineering, Newcastle University, Newcastle upon Tyne NE1 7RU, UK.

E-mail address: [sadegh.nadimi-shahraki@ncl.ac.uk](mailto:sadegh.nadimi-shahraki@ncl.ac.uk) (S. Nadimi).

In this study, a series of three-dimensional (3D) DEM simulations are conducted to investigate the effect of operating rotational speed on the system performance. Areas of interests are particle dynamics, shear band formation, compressive forces on particles, the stress generated on the push-arm and the operational energy requirements. Correlations are established between the stress, expended energy and rotational speed. The simulation process provides an understanding of the stress conditions, as particle coating is essentially by bulk powder shear straining. So, the simulation results play a guiding role in engineering practice.

## 2. Materials and methods

The Mechanofusion system comprises a rotating chamber with 100 mm internal diameter and 50 mm height and a push-arm, which is in the form of half-cylinder, with 25 mm diameter as shown in Fig. 1. There is a scraper after the push-arm in the actual system to clear the particle off the chamber wall. This is not modelled here, as it is not affecting the objectives of this study.

EDEM® software package (DEM-Solutions, Edinburgh, UK) is used for DEM simulations. The software is established based on soft sphere approach (see e.g. [16]). In these simulations, contact interactions are modelled based on Hertz-Mindlin contact laws. Spherical particles with 200 g mass, corresponding to about 153,000 particles with median diameter ( $d_{50}$ ) of 1 mm are generated with random particle size distribution in the range  $(0.8-1.2)d_{50}$ . The total mass of the particle is generated over 0.3 s for all simulations. The particle factory has dimensions  $8 \times 16 \times 25 \text{ mm}^3$  and is placed in a quadrant behind the push-arm at 12.00 o'clock position and the push-arm is at 3.00 o'clock position. The simulations are conducted using four rotational speeds of the chamber: 500, 1000, 2500, 5000 rpm. Total simulation time for each run is 0.5 s, providing sufficient window of time for the system to reach steady-state, but minimising computational time and cost. Additional simulation is conducted with a finer particle size, i.e.  $d_{50} = 0.50 \text{ mm}$  and rotational speed of 5000 rpm. The results of this simulation are used to investigate the particle size effect. All other simulation conditions are kept unchanged. The physical and mechanical properties of particles used in the simulations are given in Table 1, representing silica particles and rigid steel walls. The

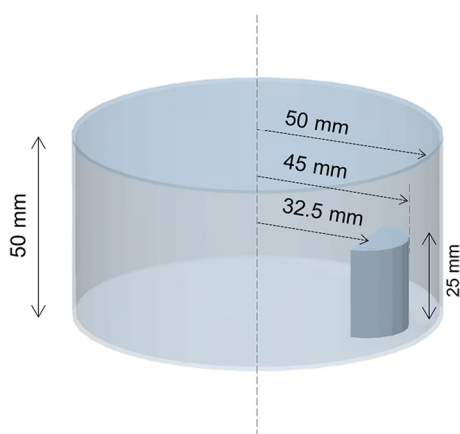


Fig. 1. The geometry of Mechanofusion without the scraper and with dimensions as measured in-house.

Table 1

Physical and mechanical properties of particles used in this study.

Simulation Parameter	Value
Particles Median Diameter [m]	0.001
Particle Density [ $\text{kg/m}^3$ ]	2500
Bulk Total Mass [kg]	0.2
Particle Shear Modulus [GPa]	0.28
Particle Young Modulus [GPa]	0.70
Particle Size Distribution	$(0.8-1.2) d_{50}$
Equipment Density [ $\text{kg/m}^3$ ]	7500
Equipment Shear Modulus [GPa]	84
Equipment Young Modulus [GPa]	210
Contact Model	Hertz-Mindlin
Coefficient of Restitution	0.5
Coefficient of Static Friction	0.5
Coefficient of Rolling Friction	0.01

integration time step for calculating particle trajectories is based on the Raleigh surface wave propagation and is  $\sim 10$  nano-second. The applicability of EDEM software for the simulation of dynamic behaviour of particles has previously been validated by Hare et al. [17] and Nan et al. [18].

The influence of the guest particles on the dynamics of the host particles is ignored in these simulations. The guest particles have indeed a profound influence on the coefficient of friction. In fact, modelling dry particle coating is a multiscale problem, as there is a large difference between the size of the host and guest particles, ranging from one to two orders of magnitude. However, the guest particles are typically either nano particles of fumed silica or fine powders, such as magnesium stearate or zeolites at low concentrations typically below 2 wt% [19,20], so that their influence is mainly on friction modification and this can be accounted for in DEM simulations by choosing appropriate value of the friction coefficient.

## 3. Results and discussion

### 3.1. Particle dynamics around the push-arm

The spatial distribution of compressive force on particles at six times ( $t = 0.03, 0.035, 0.04, 0.05, 0.1$  and  $0.5 \text{ s}$ ) for each simulation are shown in Fig. 2. A progressive change in the particle dynamics from 500 rpm to 5000 rpm can be noticed. The first analysis time is at 0.03 s. The particle bed at 2500 and 5000 rpm is so shallow that it passes through the gap between the push-arm and the wall without getting sheared. However, at 500 and 1000 rpm, the layer is considerably thicker as particle addition rate is constant, regardless of rotational speed. As a result, the accumulation of particles before the push-arm is visible in the early stage of the simulation. In the next analysis time (0.035 s), a fraction of the bed depth is shaved-off and the particles rebound with an angle depending on the speed of rotation and rate of addition of particles. Particles accumulate in front of the push arm, caused by the constricting gap, the extent of which is increased as the rotational speed is reduced. Another noticeable feature is that a thick layer is observed at low rotational speeds, due to layer experiencing lower centrifugal force as compared to larger rotational speeds.

While particles are being fed, a bigger rebound angle is detected. This is caused by the factory position and initial particle speed. Once feeding is complete and time is allowed for the feeding disturbance to subside and the system to reach steady state condition, a considerable angle shift is detected (cf. 0.5 s in Fig. 2). Here, the angle is defined

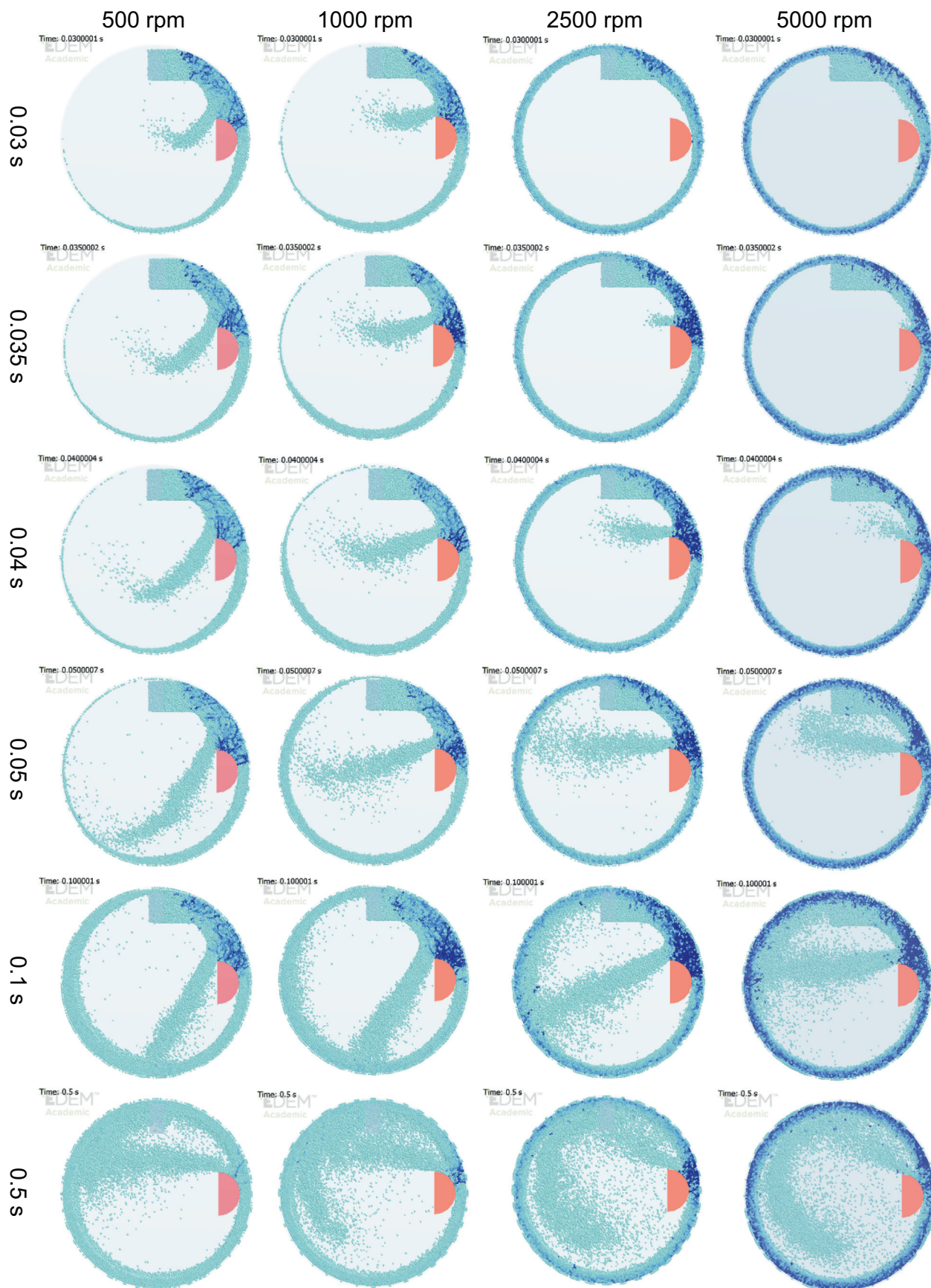


Fig. 2. Particle dynamics in MechanoFusion process at four rotational speeds and six times, compressive forces on each particle are shown by the shades of blue covering the force range from 0 to 0.5 N.

Time: 0.100001 s

EDEM Academic

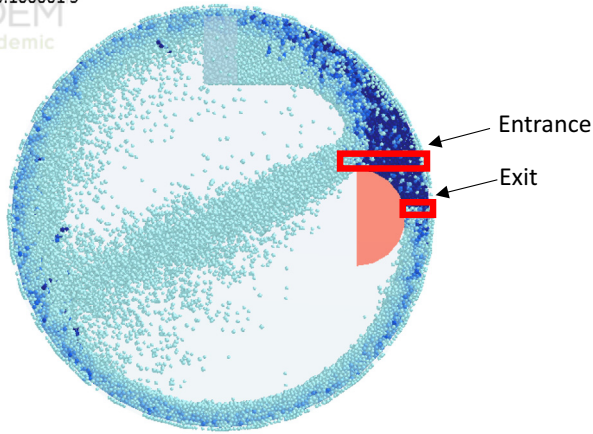
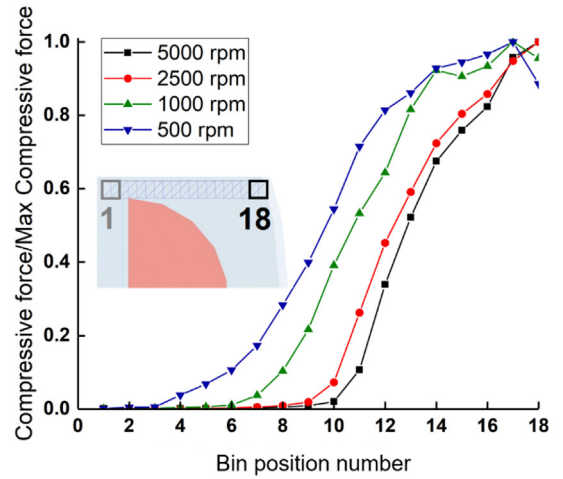
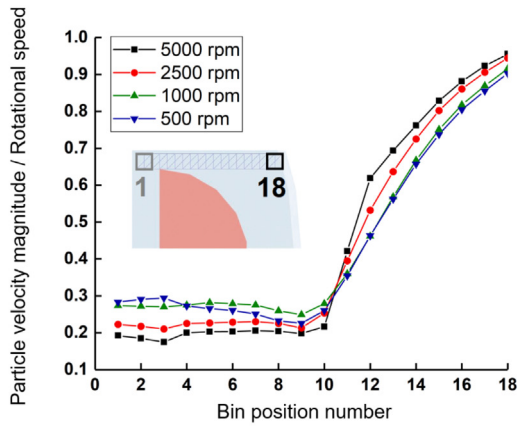


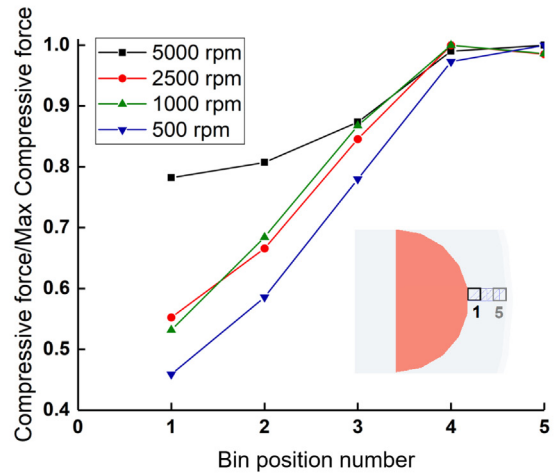
Fig. 3. Definition of entrance and exit area used in the calculation.



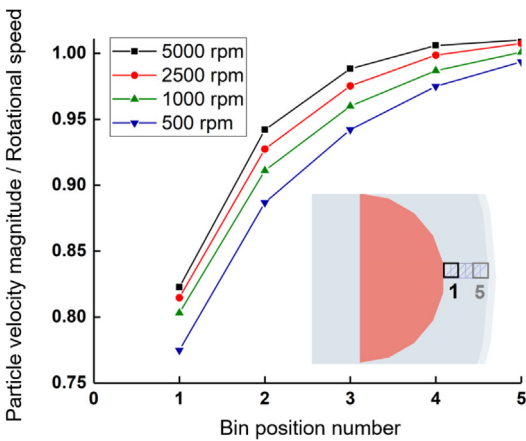
(a)



(a)



(b)



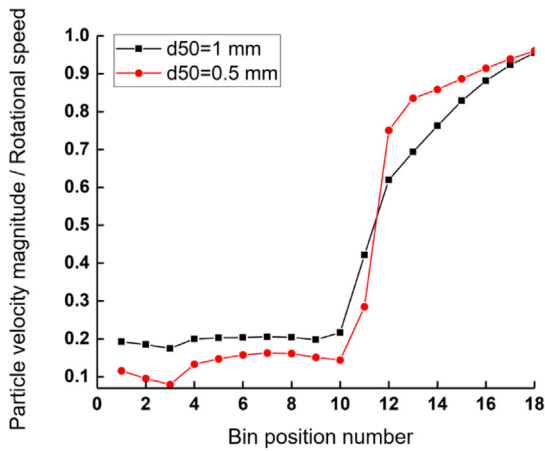
(b)

Fig. 4. Particle velocity profiles averaged over 0.3 to 0.5 s at four rotational speeds at (a) entrance and (b) exit as defined on the graph.

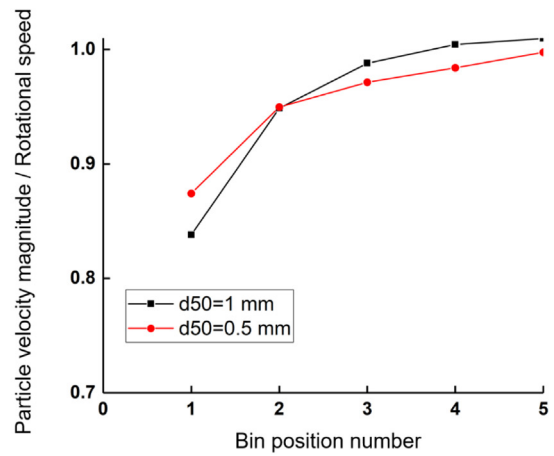
Fig. 5. Compressive force on particles at four rotational speeds at (a) entrance and (b) exit as defined on the graph.

with respect to the tangent to the particle bed free surface, i.e. a zero angle indicating no deflection. The larger the rotational speed, the bigger the rebound angle, as the particles experience a larger impact momentum. A fully developed particle bed for all rotational speeds can be observed in the final simulation stage shown in Fig. 2. A gradual reduction in the particle bed depth with increasing the rotational speed is observed, due to an increase in the packing fraction.

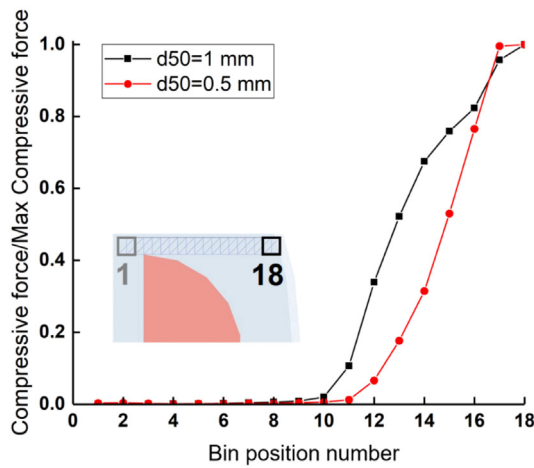
Two regions are identified for further examination: (i) the entrance region before the constricting zone created by the push-arm and the chamber wall; (ii) an exit region (Fig. 3). Particles experience the highest compression load and consequently highest shear stresses between these two positions.



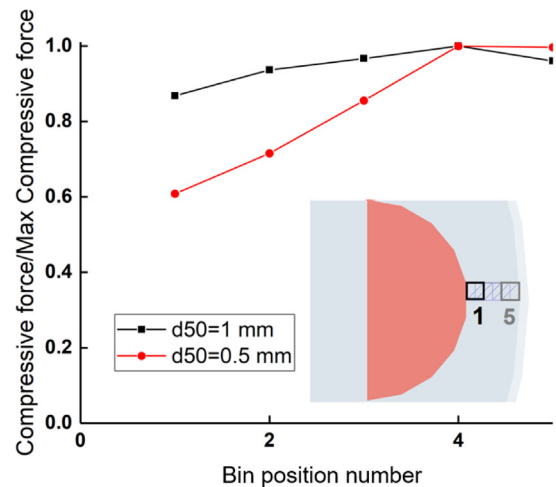
(a)



(a)



(b)



(b)

**Fig. 6.** Effect of particle size on (a) velocity and (b) compressive force profile at the entrance region.

In order to analyse the conditions in these regions, the entrance region is defined by 18 cuboid bins with the size of  $2d_{50} \times 2d_{50} \times 25$  mm. To avoid omitting particles between two successive bins, an overlap of one particle diameter, i.e. 50%, is considered. A similar approach is applied for the exit region, but a sequence of five bins is fitted to cover the segment. Particle velocity, compressive force and arm pressure are analysed in the following sub-sections after reaching steady state, from  $t = 0.3$  to  $0.5$  s, with no considerable fluctuations.

### 3.1.1. Velocity profile

The normalised velocity profile for the entrance area, illustrated in Fig. 4(a), indicates a flat unvarying and small velocity up to bin number 10, and then sharply rising, implying shearing at great strain rates from bins 10 to 18. In the first 10 bins, particle velocity is surprisingly lower for larger rotational speeds, but this trend reverses for bins 10–18, as naturally expected. High fluctuations at 500 rpm in the first 12 bins cause the average to slightly deviate from the trend. Near the wall, particle velocity approaches the rotational speed of the wall.

**Fig. 7.** Effect of particle size on (a) velocity and (b) compressive force profile at the exit.

The particle velocity profile in the exit region is shown in Fig. 4(b). At larger rotational speeds, particles attain speeds closer to those of the wall. At 5000 and 2500 rpm, particles are closer to the rotational speed ( $>80\%$ ) compared to 1000 rpm and 500 rpm ( $<80\%$ ). Furthermore, particles contacting the wall at 5000 and 2500 rpm are reaching the rotational speed of the wall, whereas at lower speeds this is not completely achieved, implying some minor slipping.

### 3.1.2. Compressive force acting on particles

Fig. 5 presents the compressive force exerted on the particles in the entrance (a) and exit (b) regions. At the entrance zone confined by the push arm and wall, the slope becomes steeper with increasing the rotational speed. Therefore, a clear boundary can be distinguished at larger velocities between the particles experiencing shear deformation in bins 10 to 18 and those relatively free from it (i.e. in bins 1–10). As previously discussed, the particle bed is shallower and denser at higher speeds and this is implied by the trend in Fig. 5(a). The forces acting on the particles in the exit region approach maximum towards the chamber wall (Fig. 5b). At 5000 rpm the whole layer is subjected to at least 80% of

maximum compression, while the compression is increasing from 40% to 100% for other rotational speed (Fig. 5b). It should be noted that the maximum compressive force is calculated separately for each rotational speed.

### 3.1.3. Particle size effect

A simulation is run at 5000 rpm with a smaller particle size than used previously ( $d_{50} = 0.5$  mm) to examine its effect on velocity distribution, the compressive force exerted on the particle bed and pressure acted on the push-arm. The results are presented in Fig. 6 and compared with those of the larger particles. Higher velocities are detected for the latter between bin 1 and 11. In the particle bed under shear deformation closer to the rotating wall (bins 12–18), the reverse effect is observed. The compressive force profile (Fig. 6b) shows similar trends for both particle sizes. However, a steeper slope is observed for the smaller particles. Consequently, a denser and shallower layer is present for the smaller particle size.

The results for the exit region are presented in Fig. 7. The finer particles contacting directly the push-arm (bin 1) have a slightly higher velocity than coarser particles. However, in the remaining part of the exit region, larger particle size shows a slightly higher velocity. The opposite situation is observed for the compressive force. A decrement with reducing the particle diameter is detected near the push-arm. Yet, at the chamber wall, the compressive force of small particles exceeds the force acted on the larger ones.

### 3.2. Stress on push-arm

The temporal profiles of the normal stress on the push-arm for all examined rotational speeds are presented in Fig. 8. The stress presented here is an averaged value, calculated from the contact forces over the front part of the push arm. At 5000 rpm, it goes through a peak at around 0.1 s, as the released particles from the factory get sheared. Once a complete layer is formed and its depth exceeds the gap width between the push-arm and the wall, it reaches an asymptotic value, albeit fluctuating, presumably due to large particles used. At 500 and 1000 rpm, the 'shaving off' of the particles by the push arm starts earlier but only lasts until the feeding is ceased. Once the particle feeding reaches completion the stress essentially stabilises. Fig. 8(b) shows a power law with an index of 1.7 fitted to the averaged pressure on the push arm versus the rotational speeds simulation.

The compressive force experienced by the particles in the compression zone takes the same shape as the pressure profiles on the push arm. It also shows a similar dependence on the rotational speed (comparing Figs. 8b and 9c). The correlation between compressive force and rotational speed gives a power-law index of 1.7. The contact force information in this zone is useful to assess the extent to which the particles might undergo attrition and breakage. For dry coating and surface modification it is important that the contact forces do not exceed the particle crushing strength. Considering Figs. 4(a), 5(a), 6(a) and 6(b) the particle velocity and compressive force build up from bin 10 to 18 (8 bins thickness) at the entrance, although there are only 5 bins at the exit region. Therefore, regardless of rotational speed, the thickness of particle bed under extreme shearing is  $8 \times d_{50}$ .

### 3.3. Power consumption of the system

The power consumption of the system is estimated from the torque data using two approaches: one based on the chamber wall, and

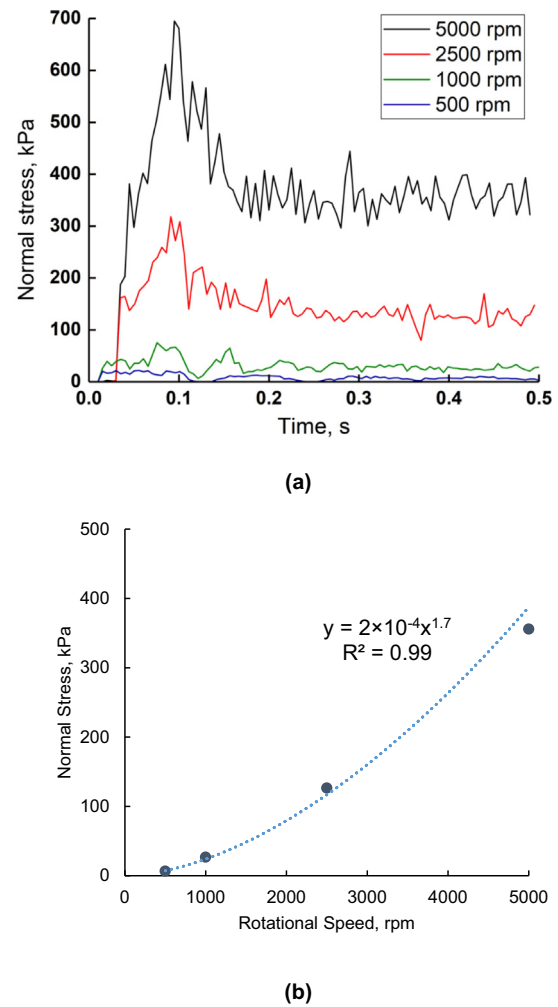


Fig. 8. Normal stress on push-arm considering compression zone only.

another based on the push-arm. For the latter, the shear stress on the surface of the push-arm is used to calculate the force and subsequently the torque on the arm, using its radius from the centre of the chamber. The results of the two calculation methods are shown in Fig. 10a and b, respectively. The input power based on the wall torque is 2.5–2.8 times higher than those based on the push-arm, as the stresses are larger there. A plot of the input power against the rotational speed is shown in Fig. 11. A power-law is fitted, which produces an index of 2.8 regardless of the calculation approach.

## 4. Concluding remarks

The particle flow pattern and associate dynamics of the Mechanofusion system were modelled using 3D DEM simulations. An adequate mass of particles was used so that the compressed layer on the rotating wall could be sheared off by the push-arm. Four rotational speeds of the wall were investigated. Qualitative visualisations of the particle flow field and of the formation of a

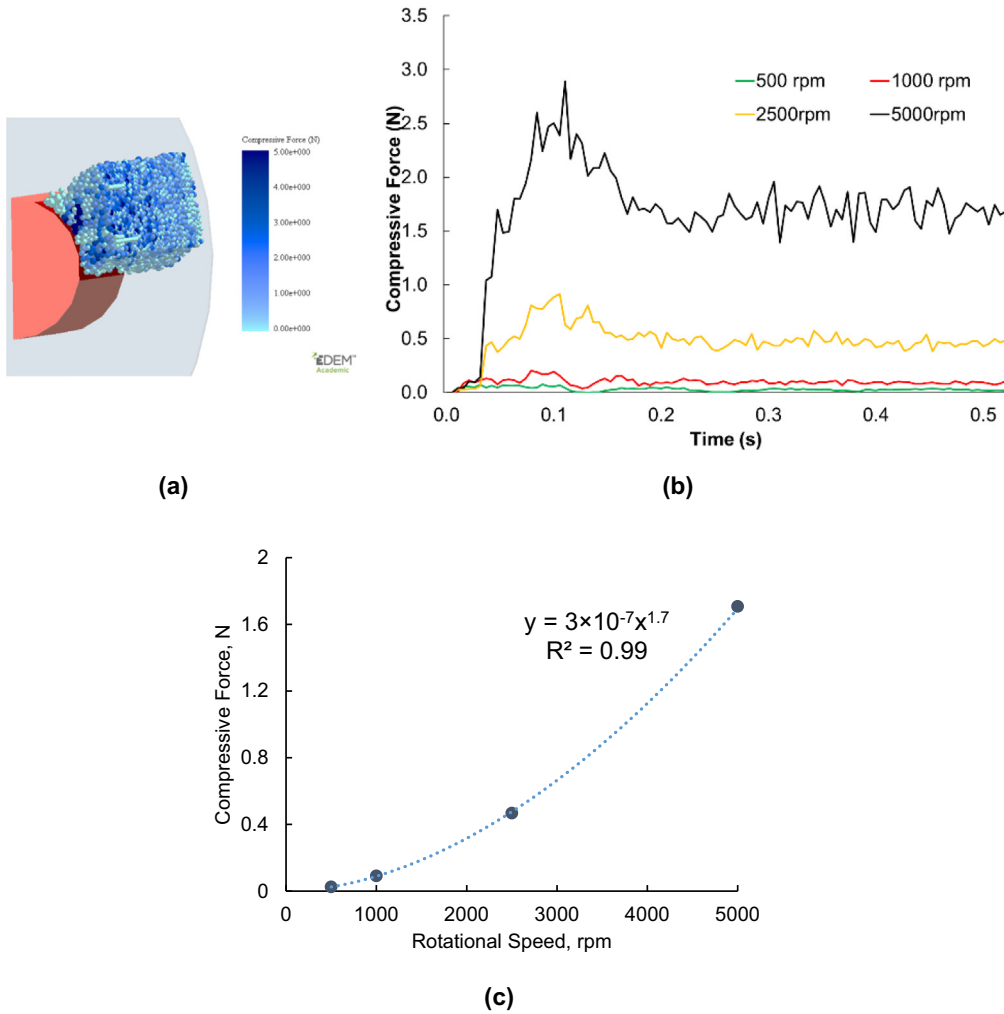
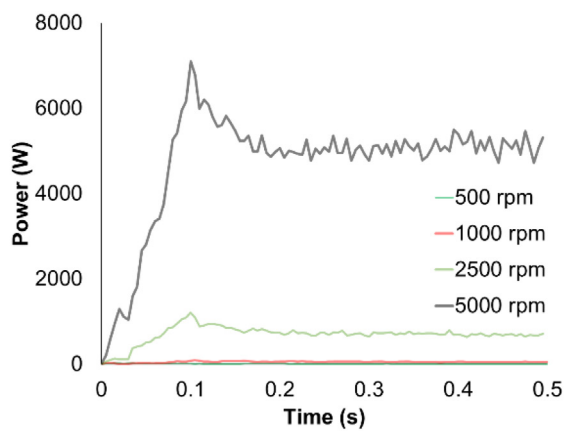


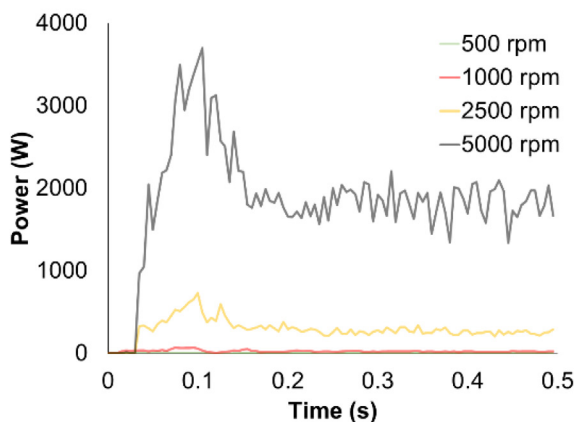
Fig. 9. (a) Illustration of compression zone, (b) compressive force profile, (c) Compressive force versus rotational speed.

particle bed on the wall were made. A quantitative analysis in terms of shear band thickness, compressive forces on particles, stress applied on the device, and input power requirement were presented. The centrifugal field produces a very large compressive contact force. The push-arm engaging with the rotating particle bed ‘shaves off’ a layer, whilst compressing the rest by the virtue of its shape, thereby generating extreme shear stresses under very large strain rates. These conditions enable efficient dry coating and ‘working’ on the particles for surface modification. It is found, regardless of

rotational speed, the thickness of particle bed under extreme shearing is  $8 \times d_{50}$ , whilst the actual gap size was  $5 \times d_{50}$ . The correlation of stress on the push-arm and rotational speed gives a power-law index of 1.7. The input power requirement is correlated to the rotational speed. A power-law fit is made, yielding an index of 2.8, regardless of calculation approach. This set-up has the potential to develop relationship and models for the rheology of powder deformation under extreme shearing rate and is the topic of interest and worthy of further work.



(a)



(b)

Fig. 10. The input power of the Mechanofusion system calculated (a) on the wall, (b) on the push-arm.

**Declaration of Competing Interest**

The authors declare that they have no known competing financial interests or personal relationships that could have appeared to influence the work reported in this paper.

**Acknowledgements**

We are grateful to Prof. Iain Crosley and Ms. Kathryn Hipkins, Hosokawa Micron Ltd. for providing access, support and information on the Mechanofusion system. We are thankful to Ms. Plamena Pencheva for her involvement in running the simulations. The support of the Engineering and Physical Sciences Research Council (grant number EP/R001766/1) as a part of ‘Friction: The Tribology Enigma’ Programme Grant ([www.friction.org.uk](http://www.friction.org.uk)) is gratefully acknowledged. We are also thankful to DEM Solutions (now Altair), Edinburgh, UK, for providing a special license for the EDEM software for use in this work.

**References**

- [1] T. Yokoyama, K. Urayama, M. Naito, M. Kato, T. Yokoyama, The angrmill mechanofusion system and its applications, *KONA Powder Part. J.* 5 (1987) 59–68.
- [2] Q.T. Zhou, L. Qu, T. Gengenbach, J.A. Denman, I. Larson, P.J. Stewart, D.A. Morton, Investigation of the extent of surface coating via mechanofusion with varying additive levels and the influences on bulk powder flow properties, *Int. J. Pharm.* 413 (1–2) (2011) 36–43.
- [3] Q.T. Zhou, L. Qu, I. Larson, P.J. Stewart, D.A. Morton, Effect of mechanical dry particle coating on the improvement of powder flowability for lactose monohydrate: a model cohesive pharmaceutical powder, *Powder Technol.* 207 (1–3) (2011) 414–421.
- [4] Matsufuji, S. and Shimizu, M., LOreal SA, (2013). Composite pigment and method for preparation thereof. U.S. Patent Application 13/983,183.
- [5] L. Zheng, C. Wei, M.D.L. Garayt, J. MacInnis, M.N. Obrovac, Spherically smooth cathode particles by mechanofusion processing, *J. Electrochem. Soc.* 166 (13) (2019) (p. A2924).
- [6] Maitra, P., Brahm, J.C., Glynn Jr, J.R., Fair, M.J. and Brown, S.E., Avon Products Inc, (2009). *Method of Improving Skin Appearance Using Treated Macroscopic Particles*. U.S. Patent Application 11/954,389.
- [7] M. Koishi, T. Ishizaka, T. Nakajima, Preparation and surface properties of encapsulated powder pharmaceuticals, *Appl. Biochem. Biotechnol.* 10 (1–3) (1984) 259–262.
- [8] M. Alonso, M. Satoh, K. Miyanami, Mechanism of the combined coating-mechanofusion processing of powders, *Powder Technol.* 59 (1) (1989) 45–52.
- [9] K. Tanno, Current status of the mechanofusion process for producing composite particles, *KONA Powder Part. J.* 8 (1990) 74–82.

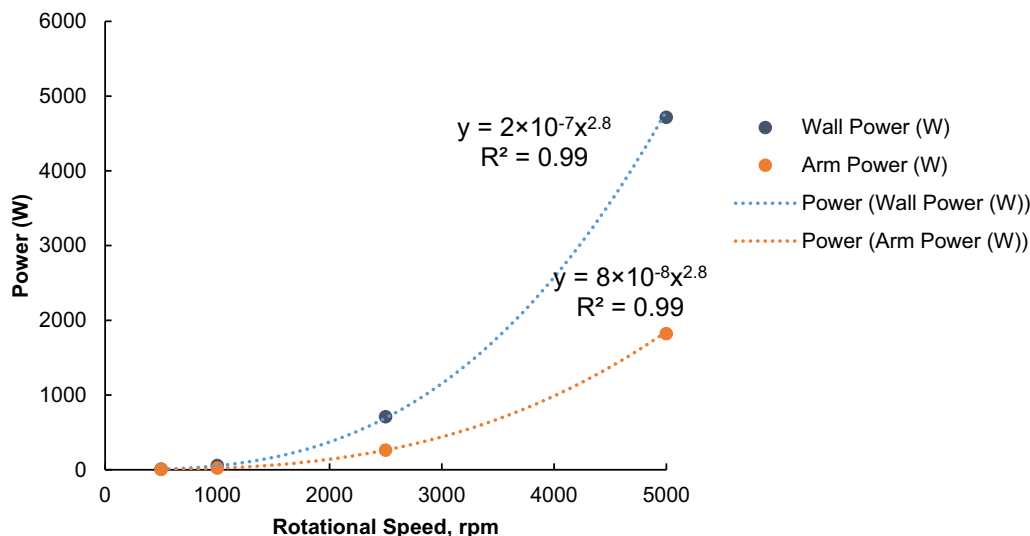


Fig. 11. The input power of the Mechanofusion system as a function of rotational speed.

- [10] M. Naito, A. Kondo, T. Yokoyama, Applications of comminution techniques for the surface modification of powder materials, *ISIJ Int.* 33 (9) (1993) 915–924.
- [11] H. Herman, Z.J. Chen, C.C. Huang, R. Cohen, Mechanofused powders for thermal spray, *J. Therm. Spray Technol.* 1 (2) (1992) 129–135.
- [12] J.Z. Chen, H. Herman, C.C. Huang, A preliminary model for mechanofusion powder processing, *KONA Powder Part. J.* 15 (1997) 113–120.
- [13] R. Pfeffer, R.N. Dave, D. Wei, M. Ramlakhan, Synthesis of engineered particulates with tailored properties using dry particle coating, *Powder Technol.* 117 (1–2) (2001) 40–67.
- [14] R. Dave, W. Chen, A. Mujumdar, W. Wang, R. Pfeffer, Numerical simulation of dry particle coating processes by the discrete element method, *Adv. Powder Technol.* 14 (4) (2003) 449–470.
- [15] W. Chen, R.N. Dave, R. Pfeffer, O. Walton, Numerical simulation of mechanofusion system, *Powder Technol.* 146 (1–2) (2004) 121–136.
- [16] C. O'Sullivan, Particle-based discrete element modeling: geomechanics perspective, *Int. J. Geomech.* 11 (6) (2011) 449–464.
- [17] C. Hare, U. Zafar, M. Ghadiri, T. Freeman, J. Clayton, M.J. Murtagh, Analysis of the dynamics of the FT4 powder rheometer, *Powder Technol.* 285 (2015) 123–127.
- [18] W. Nan, M. Ghadiri, Y. Wang, Analysis of powder rheometry of FT4: effect of particle shape, *Chem. Eng. Sci.* 173 (2017) 374–383.
- [19] F. Fulchini, U. Zafar, C. Hare, M. Ghadiri, H. Tantawy, H. Ahmadian, M. Poletto, Relationship between surface area coverage of flow-aids and flowability of cohesive particles, *Powder Technol.* 322 (2017) 417–427, <https://doi.org/10.1016/j.powtec.2017.09.013>.
- [20] Q.T. Zhou, L. Qu, T. Gengenbach, I. Larson, P.J. Stewart, D.A. Morton, Effect of surface coating with magnesium stearate via mechanical dry powder coating approach on the aerosol performance of micronized drug powders from dry powder inhalers, *AAPS PharmSciTech* 14 (1) (2013) 38–44.